MODELING THE DYNAMICS OF PARTIAL WETTING

Manuel Huber[1], Winfried Säckel[1], Manuel Hirschler[1], S. Majid Hassanizadeh[2] and Ulrich Nieken[1]

[1] Institute of Chemical Process Engineering (ICVT)
University of Stuttgart
Böblinger Str. 78, 70199 Stuttgart, Germany
Manuel.Huber@icvt.uni-stuttgart.de
http://www.icvt.uni-stuttgart.de

[2] Department of Earth Sciences, Faculty of Geosciences
Utrecht University
P.O. Box 80021, 3508 TA Utrecht, The Netherlands
http://www.geo.uu.nl/hydrogeology/

Key words: SPH, surface tension, dynamic contact angle, moving contact line, partial wetting

Abstract. The behavior of interfaces and contact lines arises from intermolecular interactions like Van der Waals forces. To consider this multi–phase behavior on the continuum scale, appropriate physical descriptions must be formulated. While the Continuum Surface Force model is well–engineered for the description of interfaces, there is still a lack of treatment of contact lines, which are represented by the intersection of a fluid–fluid interface and a solid boundary surface. In our approach we use the "non compensated Young force" to model contact line dynamics and therefore use an extension to the Navier–Stokes equations in analogy to the extension of a two–phase interface in the CSF model. Because particle–based descriptions are well–suited for changing and moving interfaces we use Smoothed Particle Hydrodynamics. In this way we are not only able to calculate the equilibrium state of a two–phase interface with a static contact angle, but also for instance able to simulate droplet shapes and their dynamical evolution with corresponding contact angles towards the equilibrium state, as well as different pore wetting behavior. Together with the capability to model density differences, this approach has a high potential to model recent challenges of two–phase transport in porous media. Especially with respect to moving contact lines this is a novelty and indispensable for problems, where the dynamic contact angle dominates the system behavior.

1 Introduction

Mass balances and momentum balances are the fundamental equations for modeling phase behavior in a wide range of chemical and mechanical processes. One usually considers bulk phases, and as long as interface phenomena are negligible, the volumetric description of the governing equation is straight forward. However, many interesting effects in multi–phase systems just happen at interfaces or even at intersections of interfaces, which are called contact lines. Balance equations can also be formulated for interfaces or contact lines, as Hassanizadeh and Gray [1] showed. If such a condition is incorporated into the governing eqations, one should be aware of the units in this condition. The balance of an interface is written in terms of an area, which has to be transformed into a volumetric description for a complete three–dimensional model. With respect to a contact line condition, a transformation from a force per line to a force per volume is necessary.

2 Two–phase model

The Navier-Stokes equations for an incompressible, Newtonian fluid in Lagrangian formulation are given by:

$$\rho \frac{D\vec{v}}{Dt} = -\nabla p + \mu \Delta \vec{v} + \rho \vec{g} \tag{1}$$

$$\frac{1}{\rho}\frac{D\rho}{Dt} = \nabla \cdot \vec{v} = 0, \tag{2}$$

where ρ, p and μ are density, pressure and dynamic viscosity. The vectors $\vec{v}$ and $\vec{g}$ represent velocity and gravitational acceleration. For a complete description of surface tension we extend (1) by two further terms:

$$\rho \frac{D\vec{v}}{Dt} = -\nabla p + \mu \Delta \vec{v} + \rho \vec{g} + \vec{F}_{wn}^{vol} + \vec{F}_{wns}^{vol}. \tag{3}$$

Here $\vec{F}_{wn}^{vol}$ represents the contribution from the interfacial balance equation, which results in the Continuum Surface Force by Brackbill et al. [3]. This force is exerted on the
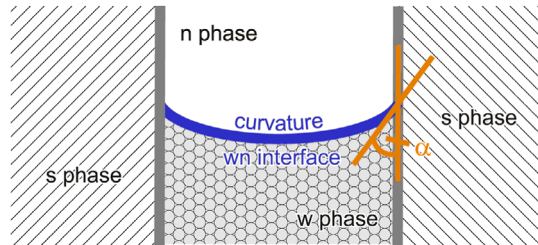

Figure 1: Two-phase system, composed of wetting (w) and non-wetting (n) phase, constrained by solid walls (s) with further key quantities: the contact angle α and the curvature κ.

wn–interface, where w denotes the wetting phase and n the non-wetting phase. With the same nomenclature we write the contribution of the momentum balance equation for a contact line as $\vec{F}_{wns}^{vol}$, where the indices wns stand for the contribution of all three phases, see fig. 1 and fig. 2.

2.1 Continuum Surface Force (CSF)

The Continuum Surface Force for a wn–interface was introduced by Brackbill et al. [3] and the result is first a force per area:

$$\vec{f}_{wn} = \sigma_{wn} \kappa_{wn} \hat{\vec{n}}_{wn}. \tag{4}$$

σ_{wn} denotes the surface tension coefficient, κ_{wn} the curvature of the wn–interface and $\hat{\vec{n}}_{wn}$ its unit normal. The normal is calculated by a weak formulation of

$$\vec{n}_{wn} = \frac{\nabla c}{[c]}. \tag{5}$$

c is the "color"-function, which is constant within each phase, but has a jump at the interface. The curvature can then be calculated through

$$\kappa_{wn} = -\nabla \cdot \hat{\vec{n}}_{wn} \tag{6}$$

and all quantities for (4) are determined. The remaining step is the volume reformulation of $\vec{f}_{wn}$, which will be explained later.

2.2 Contact Line Force (CLF)

From the *Microscale Momentum Balance Equation for a Contact Line* [1] one can derive the *unbalanced Young Force* [6]. We use this formulation as driving force for the dynamics of the contact line:

$$\vec{f}_{wns} = \left(\sigma_{ns} - \sigma_{ws} + \sigma_{wn} \underbrace{(\hat{\vec{\nu}}_{ns} \cdot \hat{\vec{\nu}}_{wn})}_{-\cos(\alpha)} \right) \hat{\vec{\nu}}_{ns}. \tag{7}$$

σ_{ij} again denotes the surface tension coefficient of the corresponding interface. The unit vectors $\hat{\vec{\nu}}_{ij}$ are defined to point away from the contact line, along the ij–interface and orthogonal to the contact line itself, see fig. 2. This formulation, where the interfacial stresses are out of balance, was already introduced by de Gennes [6]. Later on Brochard-wyart and de Gennes published a constitutive relation for the dynamic contact angle in dependence of the contact line velocity [2].
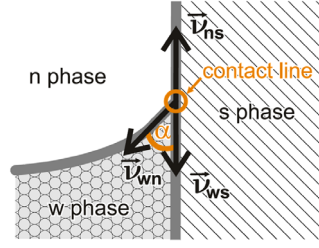
Figure 2: Contact line with contact angle α

2.3 Volume reformulation

If we consider line forces or area forces everything is fine in an analytical imagination. But when we change to a discrete, numerical formulation, we experience problems, because in three-dimensional space each discrete voxel or particle has an extension. This volume reformulation has two functions. On the one hand it "activates" the force at the region of interest, e.g. an interface, and takes care of setting the contribution to zero away from this region. On the other hand it is responsible for preserving the integral quantity of the e.g. interfacial force.

The volume reformulation of the CSF is described in [3]. In general the transformation is given by

$$\vec{F}_{wn}^{vol} = \vec{f}_{wn}\delta_{wn}, \tag{8}$$

where the Dirac delta distribution δ_{wn} is non-zero on the wn–interface and zero everywhere else. Moreover it fulfills the condition

$$\int\limits_{-\infty}^{\infty} \delta_{wn}(x - x_0)dx = 1, \tag{9}$$

to preserve the quantity. Brackbill et al. showed, that $|\vec{n}_{wn}|$, if defined by (5), can be used as numerical realization for the Delta distribution. In this way one obtains

$$\vec{F}_{wn}^{vol} = \sigma_{wn}\kappa_{wn}\vec{n}_{wn}. \tag{10}$$

In the same way we define the volume reformulation of the contact line force by

$$\vec{F}_{wns}^{vol} = \vec{f}_{wns}\delta_{wns}, \tag{11}$$

where δ_{wns} in this case is responsible for a transformation from a force per line to a force per volume and therefore fulfills the condition

$$\int\limits_{-\infty}^{\infty}\int\limits_{-\infty}^{\infty} \delta_{wns}(x - x_0, y - y_0)dxdy = 1. \tag{12}$$

3   Implementation in SPH

The basis of every SPH interpolation

$$A_a\left(\vec{r}\right) = \sum_b \frac{m_b}{\rho_b} A_b W_{ab}(\vec{r}_{ab}, h) \tag{13}$$

is the utilized smooting kernel W. Here $\vec{r}_{ab}$ denotes the disctance vector from particle b to a and h is the so-called smoothing length. Due to stability issues of cubic formulations we use the quintic spline by Wendland [12] in this two-dimensional model:

$$W\left(\vec{r}, h\right) = \frac{7}{4\pi h^2} \begin{cases} \left(1 - \frac{q}{2}\right)^4 (2q + 1) & \text{if } q < 2 \\ 0 & \text{else} \end{cases}. \tag{14}$$

This form gives rise to a more regularized particle ordering in dynamical processes compared to a cubic version. Here q is given by $q = |r|/h$.

3.1   Discretization of the Navier–Stokes equations

The pressure term in the Navier-Stokes equation is calculated using the formulation of Morris [4]:

$$\left(\frac{1}{\rho}\nabla p\right)_a = \sum_b m_b \frac{p_a + p_b}{\rho_a \rho_b} \nabla_a W_{ab}. \tag{15}$$

This was later also used by Colagrossi & Landrini [7]. The viscous formulation is taken from Szewc et al. [5]:

$$\left(\nabla(\eta\nabla\cdot\vec{v})\right)_a = \sum_b 8m_b \frac{\eta_a + \eta_b}{\rho_a + \rho_b} \frac{\vec{v}_{ab}\cdot\vec{r}_{ab}}{|\vec{r}_{ab}|^2 + \zeta^2} \nabla_a W_{ab}, \tag{16}$$

where $\eta = \mu/\rho$ is the kinematic viscosity and $\vec{v}_{ab} = \vec{v}_a - \vec{v}_b$ is the velocity difference of particle a and b. $\zeta = 0.01h$ is a small numerical parameter, preventing the denominator to become zero. The density is calculated in the way of Hu & Adams [8]:

$$\rho_a = m_a \sum_b W_{ab}. \tag{17}$$

Although this formulation is not variational consistent according to Bonet & Lok [9], the result is in good agreement with some verifications we made.

3.2   Surface tension formulation

In this paper we use the CSF formulation of Morris [4]. This approach does not conserve linear and angular momentum, but is well–known for its stability [11]. Therefore following

equations are utilized:

$$\vec{n}_{wn_a} = \frac{1}{[c]} \sum_b \frac{m_b}{\rho_b} \left(c_b - c_a\right) \nabla_a W_{ab} \tag{18}$$

$$\kappa_{wn_a} = -\sum_b \frac{m_b}{\rho_b} \left(\hat{\vec{n}}_{wn_b} - \hat{\vec{n}}_{wn_a}\right) \cdot \nabla_a W_{ab} \tag{19}$$

$$\vec{F}_{wn_a}^{vol} = \sigma_{wn} \kappa_{wn_a} \vec{n}_{nw_a}. \tag{20}$$

In the case of the CLF, the volume reformulation δ_{wns} is composed of

$$\delta_{wns_a} = \frac{1}{N_a} |\vec{n}_{wn_a}| W_{as}\left(d_s, h\right), \tag{21}$$

where d_s is the distance to the solid wall and N_a is the normalization constant, which preserves the integral quantity of the CLF in this two-dimensional problem by

$$N_a = \sum_b \frac{m_b}{\rho_b} |\vec{n}_{wn_a}| W_{as}\left(d_s, h\right). \tag{22}$$

This integration has to be done over one complete contact line area and results in the volumetric description of the CLF:

$$\vec{F}_{wns_a}^{vol} = \left(\sigma_{ns} - \sigma_{ws} + \sigma_{wn} \underbrace{(\hat{\vec{\nu}}_{ns_a} \cdot \hat{\vec{\nu}}_{wn_a})}_{-\cos(\alpha)}\right) \hat{\vec{\nu}}_{ns_a} \, \delta_{wns_a}. \tag{23}$$

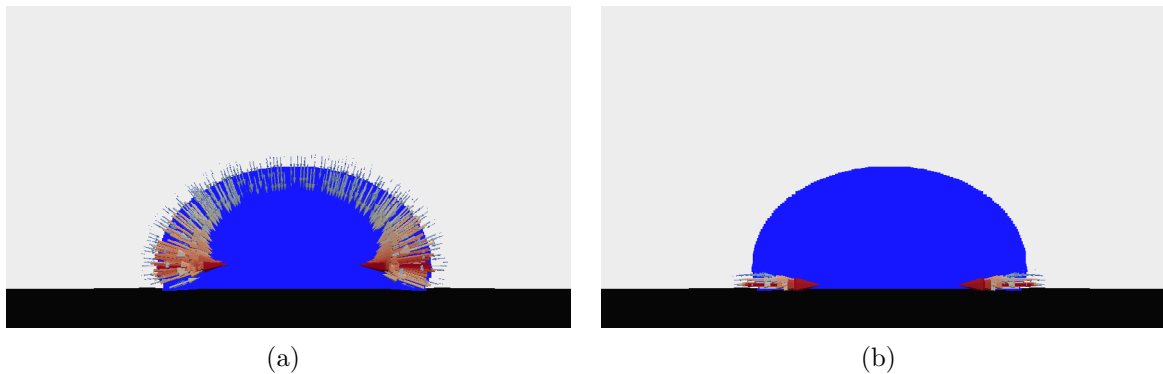In this way we get the forces which are responsible for wetting of a solid surface and

Figure 3: Droplet shape on a solid wall under the influence of surface tension, a balance for the contact line, and gravity with a density ratio of 1:10. Arrows show a random set of particles with (a) Continuum Surface Force and (b) Contact Line Force.

the dynamics of interfaces, see fig. 3. The idea of this approach is to decouple wetting dynamics from interface dynamics and obtain two different descriptions. This is advantageous, because in many technical applications the wetting dynamics vary, and hereby one is able to either exchange the driving force $\vec{f}_{wns}$ or the volume reformulation δ_{wns} to utilize different wetting models.

3.3 Time integration

To ensure incompressibility and avoid fitting parameters, a predictor–corrector scheme after Shao & Lo [10] is applied, following the projection method of Chorin [15]. By this means one first accomplishes the predictor step, which moves the particles according to viscosity and external forces with an explicit Euler method. In this way the intermediate particle position is given by

$$\vec{r}_{int} = \vec{r}_t + \vec{v}_{int}\Delta t \tag{24}$$

with $\vec{v}_{int}$ beeing the intermediate particle velocity, defined by

$$\vec{v}_{int} = \left(\eta\Delta\vec{v}_t + \vec{g} + \frac{1}{\rho}\vec{F}_{wn}^{vol} + \frac{1}{\rho}\vec{F}_{wns}^{vol} \right)\Delta t + \vec{v}_t. \tag{25}$$

$\vec{r}_t$ and $\vec{v}_t$ are position and velocity of the last complete time step and Δt is the discrete time step interval. To accomplish the corrector step, the following remaining term of the momentum balance is used

$$\vec{v}_{t+1} = \left(-\frac{1}{\rho}\nabla p_{t+1} \right)\Delta t + \vec{v}_{int}, \tag{26}$$

where p_{t+1} is the pressure of the next time step. Thus the complete step is made by

$$\vec{r}_{t+1} = \vec{r}_t + \left(\frac{\vec{v}_t + \vec{v}_{t+1}}{2} \right)\Delta t. \tag{27}$$

3.3.1 Incompressible formulation

Equation (2) demands the divergence–free velocity field of the complete time step

$$\nabla \cdot \vec{v}_{t+1} = 0. \tag{28}$$

In this manner by taking the divergence of (26) and using (28), we obtain the pressure Poisson equation

$$\nabla \cdot \left(\frac{1}{\rho}\nabla p_{t+1} \right) = \frac{\nabla \cdot \vec{v}_{int}}{\Delta t}, \tag{29}$$

which is a condition for the pressure to result in an approximate incompressible fluid behavior of the whole system. This step couples the entire domain in a LES. We follow

the formulation of Cummins & Rudman [13], where the LHS of the LES is calculated by

$$\left(\nabla \cdot \left(\frac{1}{\rho}\nabla p\right)\right)_a = \sum_b \frac{m_b}{\rho_b}\frac{4}{\rho_a + \rho_b}\frac{p_{ab}\vec{r}_{ab} \cdot \nabla_a W_{ab}}{|\vec{r}_{ab}|^2 + \zeta^2}. \tag{30}$$

p_{ab} denotes the pressure difference $p_{ab} = p_a - p_b$. The RHS of (29) is given by

$$\left(\frac{\nabla \cdot \vec{v}_{int}}{\Delta t}\right)_a = \frac{1}{\Delta t}\sum_b \frac{m_b}{\rho_b}\left(\vec{v}_{int_b} - \vec{v}_{int_a}\right) \cdot \nabla_a W_{ab}. \tag{31}$$

3.4 Boundary conditions

On top a no-slip Dirichlet BC is applied for the velocity and a Neumann BC is applied for the pressure

$$|\vec{v}|\bigg|_{top} = 0 \tag{32}$$

$$\frac{dp}{dn}\bigg|_{top} = 0 \quad . \tag{33}$$

This is realized with image particles, reflected at the domain boundary, with the properties:

$$p_{a'} = p_a \quad \text{and} \quad \vec{v}_{a'} = -\vec{v}_a \ . \tag{34}$$

On the left and right domain boundary, periodic BCs are implemented. A no-slip condition is applied at the solid–fluid interface in accordance to Morris et al.[14] and the pressure Poisson equation is also solved on solid particles at the bottom wall. In this manner an extrapolated pressure gradient is obtained, which prevents the particles from penetrating the wall, even with a remaining force contribution normal to the wall.

4 Results

This approach is well-suited to model dynamic processes. In the first instance we look at a less dynamical test case. Starting with an initial phase distribution as shown in fig. 4(a), we obtain the evolution of the system until the final equilibrium state is reached, see fig. 4(b). The calculation is performed with a static contact angle of 40°. More interesting investigations however, can be made under dynamical conditions. Therefore we model the detachment of a droplet in a gas channel as shown in fig. 5. An inflow condition is simulated so that for incompressible fluids, the inflowing mass flux equals the outflowing mass flux. In this manner, with periodic boundary conditions, expensive memory management can be avoided and only the velocity field for particles close to the inlet has to be reinitialized according to the inflow/outflow condition. In this way we look at advancing and receding contact angles of a moving drop. Lam et al. [17] made comparable experiments, where they studied advancing contact angles of different alkanes
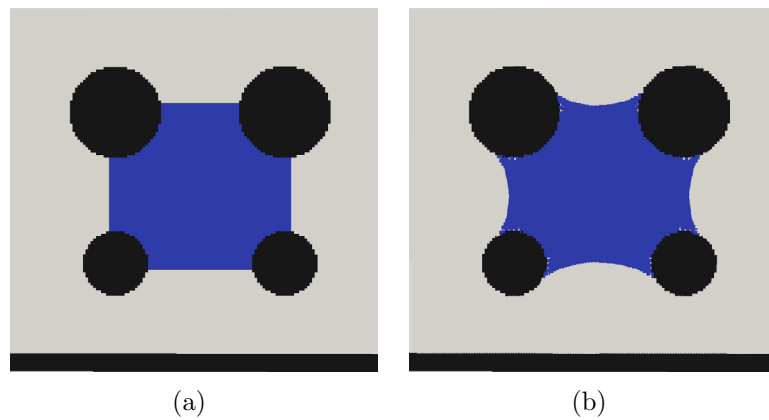
(a)   (b)

Figure 4: (a) Initial phase distribution, confined by four solid spheres. (b) Equilibrium state for a wetting fluid with a static contact angle of 40°.
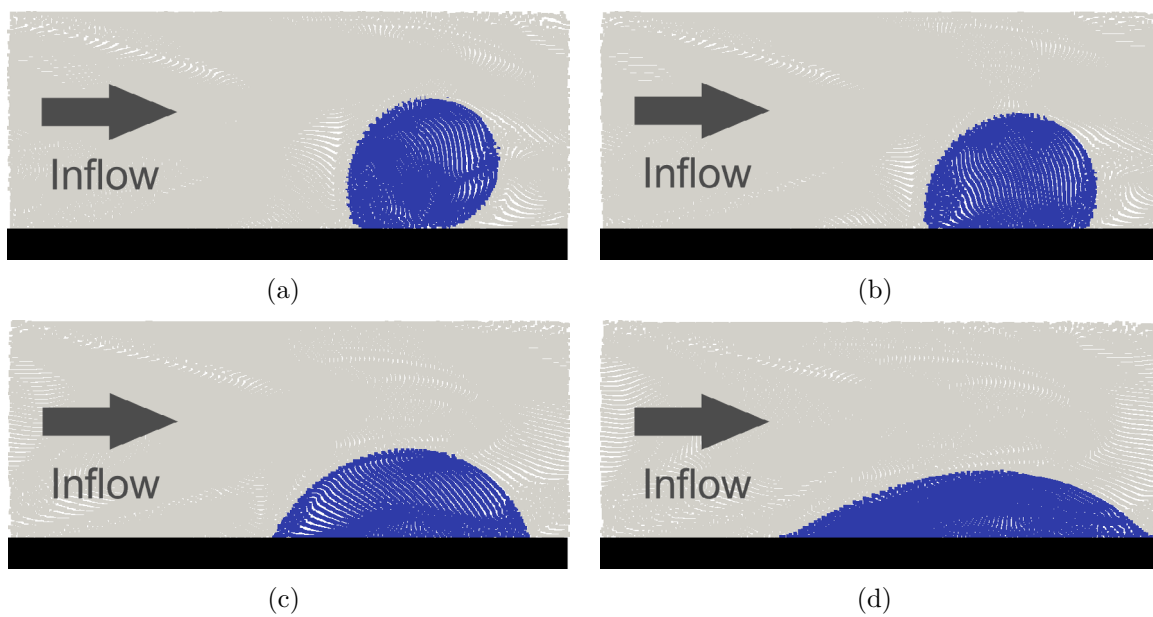

(a)   (b)

(c)   (d)

Figure 5: Detachment of a droplet with inflow and outflow condition in a channel with different static contact angles of (a) 40°, (b) 70°, (c) 110° and (d) 140°. Different advancing and receding contact angles are the apparent result.

on a coated silicon wafer by constantly injecting the alkane through a needle into a resting drop. Hence the volume of the drop rises and the contact line is pushed away from the injecting needle, resulting in an advancing contact angle α_{adv}. In the same way receding contact angles α_{rec} were investigated by decreasing the drop volume. Results are shown in table 1. For comparison, the setup of the simulation was chosen as shown in fig. 5

with an inlet velocity of $\vec{v}_{in} = 0.02 \ m/s$. The surface tension coefficients are calculated from the experimental data of Lam et al. using the equations of Tadmor [16], see table 1. Hereby advancing and receding contact angles are obtained at once. Fig. 6 shows the accordance of the SPH model with the experiments of Lam et al.
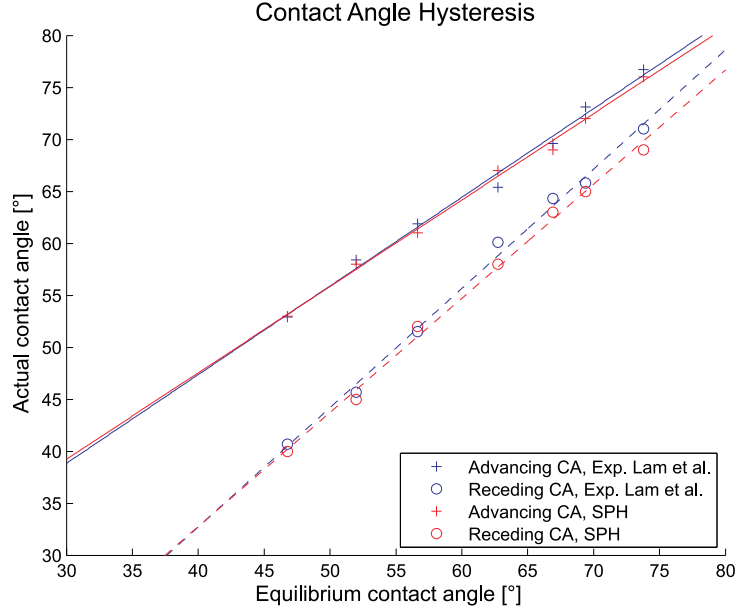

Figure 6: Contact angle hysteresis. Cross marker denote experiment/simulation of advancing contact angle, circular marker represent the receding contact angle. Experiment of Lam et al. [17] in blue, SPH simulation in red. Straight and dashed lines are fitted straight lines.

Table 1: Experimental results from Lam et al. [17], further evaluated with the formulation of Tadmor [16], to obtain static contact angle α_{stat} and surface tension coefficient $\sigma_{xs} = \sigma_{ns} - \sigma_{ws}$.

Liquid	$\sigma_{wn} \ [N/m]$	$\sigma_{xs} \ [N/m]$	$\alpha_{adv} \ [°]$	$\alpha_{rec} \ [°]$	$\alpha_{stat} \ [°]$
n-Hexane	0.0182	≈ 0.0124	52.9	40.7	≈ 46.8
n-Heptane	0.0200	≈ 0.0123	58.4	45.7	≈ 52.0
n-Octane	0.0214	≈ 0.0118	61.9	51.5	≈ 56.6
n-Nonane	0.0226	≈ 0.0104	65.4	60.1	≈ 62.7
n-Undecane	0.0244	≈ 0.0096	69.6	64.3	≈ 66.9
n-Tridecane	0.0258	≈ 0.0091	73.1	65.8	≈ 69.4
n-Hexadecane	0.0276	≈ 0.0077	76.7	71.0	≈ 73.8

5 Conclusions

In this paper we show how momentum balances at interfaces and contact lines can be incorporated into existing Navier–Stokes models by using a volume reformulation. The advantage with respect to surface tension modeling is, that in this approach, different wetting models can be utilized. This approach is capable of describing dynamic contact angles and in the presence of a drag force it describes droplet movement with accompanying advancing and receding contact angles. The model was validated by experimental results.

Acknowledgment

REFERENCES

[1] S. M. Hassanizadeh, W. G. Gray, Thermodynamic basis of capillary pressure in porous media, Water Resources Research 29 (10) (1993) 3389–3405.

[2] F. Brochardwyart, P. G. de Gennes, Dynamics of partial wetting, Advances In Colloid and Interface Science 39 (1992) 1–11.

[3] J. U. Brackbill, D. B. Kothe, C. Zemach, A continuum method for modeling surface tension, Journal of Computational Physics 100 (2) (1992) 335–354.

[4] J. P. Morris, Simulating surface tension with smoothed particle hydrodynamics, International Journal For Numerical Methods In Fluids 33 (3) (2000) 333–353.

[5] K. Szewc, J. Pozorski, J.–P. Minier, Analysis of the incompressibility constraint in the smoothed particle hydrodynamics method, International Journal For Numerical Methods In Engineering 92 (2012) 343–369.

[6] P. G. de Gennes, Wetting - Statics and Dynamics, Reviews of Modern Physics 57 (3) (1985) 827–863.

[7] A. Colagrossi, M. Landrini, Numerical simulation of interfacial flows by smoothed particle hydrodynamics, Journal of Computational Physics 191 (2003) 227–264.

[8] X. Hu, N. Adams, A multi–phase sph method for macroscopic and mesoscopic flows, Journal of Computational Physics 213 (2) (2006) 844–861.

[9] J. Bonet, T. S. L. Lok, Variational and momentum preservation aspects of Smooth Particle Hydrodynamic formulations, Computer Methods In Applied Mechanics and Engineering 180 (1–2) (1999) 97–115.

[10] S. Shao, E. Y. M. Lo, Incompressible sph method for simulating newtonian and non-newtonian flows with a free surface, Advances in Water Resources 26 (7) (2003) 787–800.

[11] K. Szewc, A. Taniere, J. Pozorski, and J. P. Minier, A Study on Application of Smoothed Particle Hydrodynamics to Multi–Phase Flows, International Journal of Nonlinear Sciences and Numerical Simulation 13 (2012) 383–395

[12] H. Wendland, Piecewise polynomial, positive definite and compactly supported radial functions of minimal degree, Advances in Computational Mathematics 4 (1995) 389–396.

[13] S. J. Cummins, M. Rudman, An sph projection method, Journal of Computational Physics 152 (2) (1999) 584–607.

[14] J. P. Morris, P. J. Fox, Y. Zhu, Modeling low reynolds number incompressible flows using sph, Journal of Computational Physics 136 (1) (1997) 214–226.

[15] A. J. Chorin, Numerical Solution of the Navier–Stokes Equations, Mathematics of Computation 22 (104) (1968) 745–762.

[16] R. Tadmor, Line energy and the relation between advancing, receding, and young contact angles, Langmuir 20 (18) (2004) 7659–7664.

[17] C. N. C. Lam, R. Wu, D. Li, M. L. Hair, A. W. Neumann, Study of the advancing and receding contact angles: liquid sorption as a cause of contact angle hysteresis, Advances In Colloid and Interface Science 96 (2002) 169–191.